Science Advances
AAAS

# Supplementary Materials for

## Nutrient management offsets the effect of deoxygenation and warming on nitrous oxide emissions in a large US estuary

Weiyi Tang *et al.*

Corresponding author: Weiyi Tang, weiyitang@usf.edu

*Sci. Adv.* **10**, eadq5014 (2024)
DOI: 10.1126/sciadv.adq5014

**This PDF file includes:**

# Supplementary text

## Biogeochemical properties of sampling stations

The two sampling stations in the seasonally hypoxic region of the bay had similar hydrographic features: fresher water in the surface overlying saltier deep water (Fig. S1), ranging in salinity from 10 to 20 across the 20 m depth profile, while temperature averaged ~26℃. However, there were large differences in the concentrations of $O_2$, $N_2O$ and dissolved inorganic nitrogen between the two stations. Station CB1.5 had a shallower oxycline and thicker anoxic layer starting at ~10 m while the anoxic layer at CB2 started at ~13 m.

$N_2O$ concentrations at CB1.5 decreased with depth and reached undersaturation in the bottom water while $N_2O$ concentrations at CB2 increased with depth and were oversaturated compared to the atmospheric equilibrium concentration. Ammonium accumulated up to 11 μM at CB1.5, with urea, nitrite, and nitrate concentrations below 1 μM. In contrast, nitrite was the dominant nitrogen nutrient at CB2, reaching up to 4 μM. The different biogeochemical properties between the two stations likely reflect the biogeochemical processes occurring during different stages of hypoxia/anoxia or influences from surrounding waters. For example, early development and long duration of low oxygen conditions at CB1.5 likely removed nitrite and nitrate in the bottom water while producing ammonium via denitrification and other nitrogen cycling processes. Low oxygen inhibited ammonia oxidation leading to the accumulation of ammonium. In contrast, dissolved inorganic nitrogen concentrations at CB2 indicate an earlier phase or shorter duration of denitrifying conditions because nitrite and nitrate have not been fully removed.

## Model evaluation and limitations

Regional Ocean Modeling System for Chesapeake Bay with Estuarine-Carbon-Biogeochemistry component (ROMS-ECB) has been shown to generally capture the spatiotemporal distributions of observed temperature, salinity, dissolved inorganic nitrogen, $O_2$ and other environmental variables in previous model evaluation studies (*29, 31*). Here we evaluated the model performance of the new $N_2O$ state variable included in ROMS-ECB by comparing modeled depth profiles of $N_2O$ concentrations with 291 data points of observed $N_2O$ concentrations in Chesapeake Bay during the summer from this study and previous studies (*12, 13, 47*). There were large spatiotemporal variations in the modeled distribution of $N_2O$ concentrations (Fig. S7). Modeled $N_2O$ concentrations at CB1.5 were generally higher than observed, likely due to the overestimated oxygen concentrations in the model (Fig. S8). The temporal mismatch may also help to explain the difference between models and observations (monthly mean for the model while summer averages from limited observations). At station CB1.75, located between CB1.5 and CB2 (Fig. S12), where modeled oxygen was closer to observations, the modeled $N_2O$ concentrations also better matched observations – slightly higher than the equilibrium concentration in surface oxygenated waters and undersaturation in the bottom low oxygen waters (Fig. S8). As for station CB2, both modeled depth profiles of oxygen and $N_2O$ concentrations were consistent with observations, successfully reproducing the observed subsurface $N_2O$ peak. Overall, the vertical distribution of $N_2O$ concentrations could be explained by the distribution of $N_2O$ cycling rates. For instance, net positive $N_2O$ production when oxygen concentration was roughly above 20 μM led to $N_2O$ accumulation while net $N_2O$ consumption in low oxygen waters led to $N_2O$ undersaturation (Fig. S12). Unfortunately, $N_2O$ concentrations in other seasons couldn't be evaluated due to the

lack of observations, highlighting the necessity for seasonal observations of $N_2O$ concentrations and cycling processes.

Although our process-based mechanistic parameterizations of $N_2O$ cycling captured the $N_2O$ distribution well, there are still a few aspects of the model that could be improved. Previous modeling studies have showed the contribution of sedimentary $N_2O$ production to inland water $N_2O$ emissions (*18, 66*). Sedimentary $N_2O$ production in our study is parameterized as a function of nitrification-denitrification (N loss) and $N_2O$ production yield (0.1%), which represents the net $N_2O$ flux from the sediment to the water column (Fig. S13). However, aquatic sediments have been observed to be either sources (*83*) or sinks of $N_2O$ (*84*). Sedimentary $N_2O$ production yield varies substantially (ranging from 0 to over 5% across aquatic sediments) and estuarine sediments generally have lower $N_2O$ production yields compared to soils, streams, and other ecosystems (*85, 86*). Sedimentary $N_2O$ yield could be affected by the availability of nitrate, organic matter, and many other environmental factors. For example, sediments in Narragansett Bay with low nitrate concentrations are often associated with low $N_2O$ yields (*84*). Sedimentary $N_2O$ production and yield in Chesapeake Bay are largely unknown due to a lack of observations, but may be closer to those in Narragansett Bay since both regions have a similar range of dissolved inorganic nitrogen concentrations and have also experienced managed nutrient reductions (*87, 88*). Thus, we applied a sedimentary $N_2O$ production yield (0.1%), which was previously observed in Narragansett Bay (*86*). A higher sedimentary yield (1%) increased the sedimentary $N_2O$ production and flux to the Chesapeake Bay water column (see Model sensitivity analysis where 1% sedimentary $N_2O$ production yield was used for comparison). However, current observations of vertical $N_2O$ profiles in the water column do not suggest a large sedimentary source contributing to the air-sea $N_2O$ flux because $N_2O$ concentrations do not always increase with depth (*12, 13, 47*). Future observations of sedimentary $N_2O$ cycling are needed to constrain the role of sediments in $N_2O$ emissions in Chesapeake Bay.

In addition, our model does not include an explicit representation of riverine $N_2O$ cycling processes since the model domain is limited to Chesapeake Bay. We prescribed the riverine $N_2O$ concentration using previous observations in the Potomac River (*79, 89*) and scaled its temporal change along with the atmospheric $N_2O$ variation over time. Overall, the riverine $N_2O$ input and its changes over time are much smaller than internal $N_2O$ cycling fluxes via nitrification and denitrification in Chesapeake Bay. In addition, a recent study found denitrification could contribute to $N_2O$ production in oxygenated coastal waters (*53*). However, our model could not resolve this phenomenon due to the parameterization of denitrification's oxygen sensitivity (i.e., denitrification is restricted at high oxygen concentration). Although previous studies have shown that $N_2O$ production by denitrification was minimal compared to the $N_2O$ production by nitrification in the oxygenated Chesapeake Bay (*13, 48*), $N_2O$ production by denitrification in oxygenated estuarine waters should be considered in future model development. Overall, despite the uncertainties in the magnitude/flux of different $N_2O$ cycling processes due to model uncertainties, the sign of changes in $N_2O$ emissions of Chesapeake Bay in response to deoxygenation, warming, and nutrient reduction would likely be the same (i.e., an increase in $N_2O$ production under deoxygenation and warming while a decrease following the nutrient reduction).

## Model sensitivity analysis

We performed sensitivity analyses to evaluate the variations in modeled $N_2O$ concentrations/fluxes in response to choices of different model input parameters. Specifically, we varied $N_2O$ production yield from nitrification using the yield derived from marine oxygen minimum zones (*35*), the oxygen sensitivity of denitrification (*90*), the rate constant for $N_2O$ reduction, the sedimentary $N_2O$ production yield, and the amount of nutrient reduction (Table S9). A lower $N_2O$ production yield from nitrification led to lower $N_2O$ concentrations and emissions (Fig. S14 and Table S9). In contrast, $N_2O$ concentrations and emissions increased substantially if denitrification was allowed to occur at a higher oxygen concentration. A smaller $N_2O$ reduction constant increased $N_2O$ concentrations and emissions as expected. $N_2O$ emissions increased substantially when a higher sedimentary $N_2O$ production yield was implemented. Finally, a smaller nutrient reduction in 2050 led to a smaller decrease in $N_2O$ emissions (133 Mg N $yr^{-1}$ when achieving half of the TMDL goal vs 124 Mg N $yr^{-1}$ when fully achieving the TMDL goal). Overall, $N_2O$ concentrations and emissions are sensitive to the choice of model parameters (particularly the oxygen sensitivity of $N_2O$ production from denitrification and sedimentary $N_2O$ production yield), emphasizing the need of targeted observations to constrain the responses of $N_2O$ cycling processes to oxygen and other environmental factors. For the analysis reported in the main text, we selected the combination of parameters best reproducing the observed $N_2O$ concentrations for estimating $N_2O$ budgets and emissions in current and future scenarios.

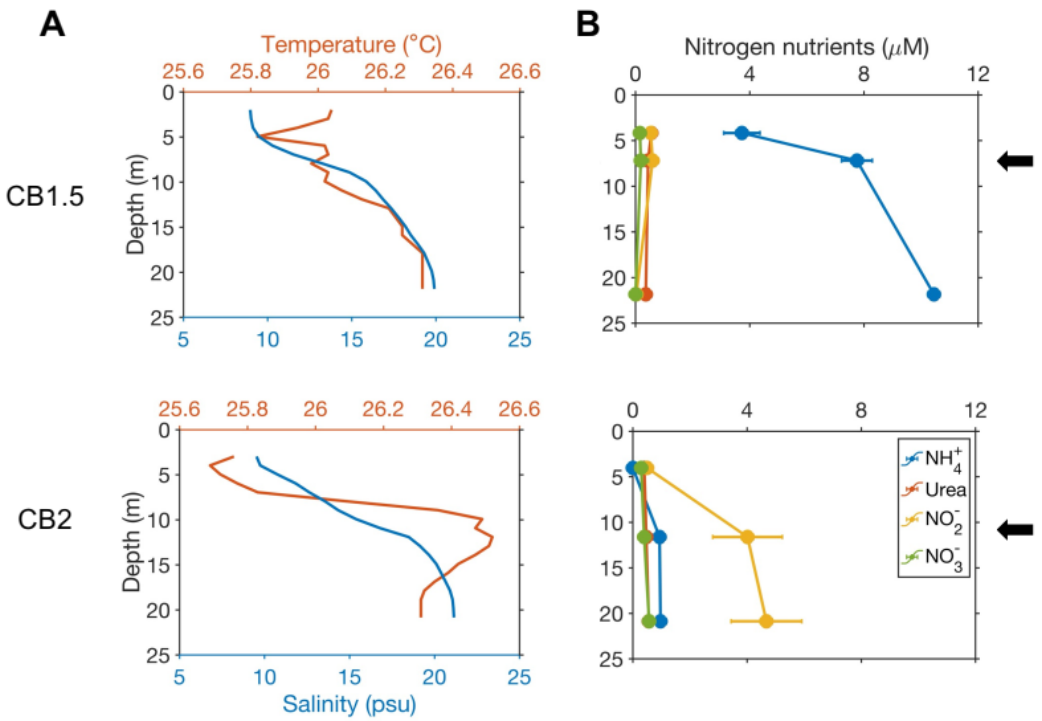


**Fig. S1. Observed biogeochemical properties of the two sampling stations.** (**A**) vertical distributions of temperature (red line) and salinity (blue line). (**B**) vertical distributions of N nutrient concentrations (blue line for $NH_4^+$, red line for urea, yellow line for $NO_2^-$, green line for $NO_3^-$). Black arrows show the depths where incubation samples were collected.

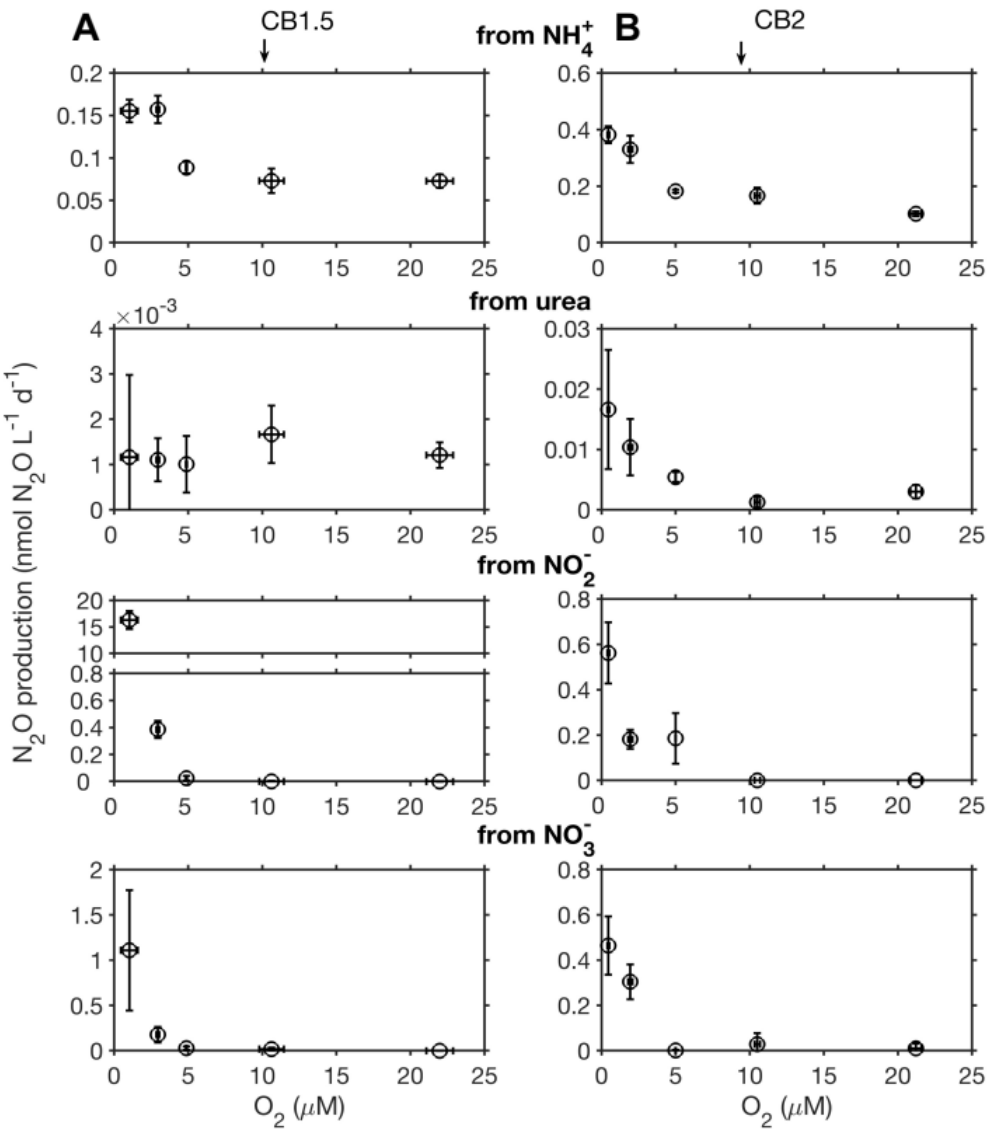


**Fig. S2. $N_2O$ production from four N substrates in response to the manipulated $O_2$ changes for samples collected at stations CB1.5 (A) and CB2 (B).** Arrows on the top panels denote in-situ oxygen concentrations at two stations. Vertical error bars represent the uncertainty of linear regression of $^{15}N$-$N_2O$ production during the incubation time course. Horizontal error bars represent variations of oxygen concentrations during the incubations.

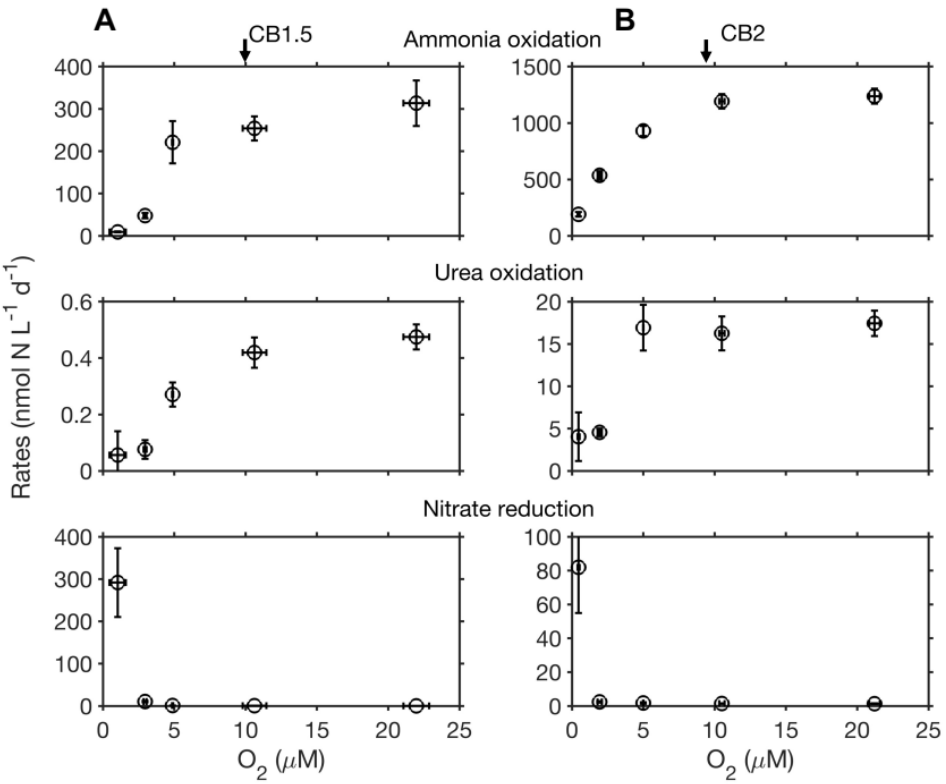


**Fig. S3. Nitrite production rate from nitrification (ammonia oxidation and urea oxidation) and denitrification (nitrate reduction) in response to manipulated $O_2$ changes for samples collected at stations CB1.5 (A) and CB2 (B).** Arrows on the top panels denote in-situ oxygen concentrations at two stations.

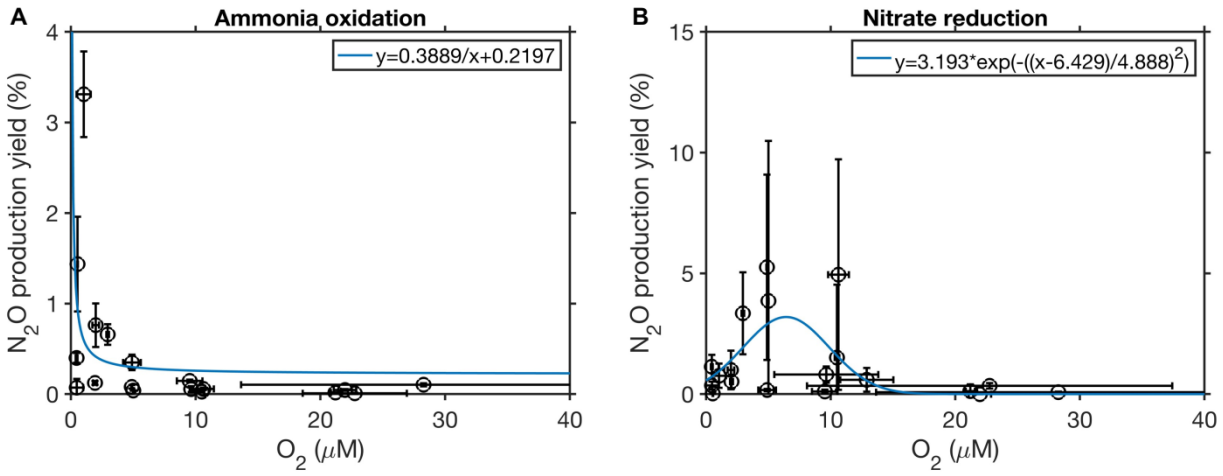


**Fig. S4. The measured $N_2O$ production yields and fitted curves in response to oxygen concentration changes from ammonia oxidation (A) and nitrate reduction (B).** The extremely high yield at 25.7% for nitrate reduction at 1.94 μM $O_2$ at CB2 is not included in subplot (**B**). Data were combined from this study and Tang et al. (2022) (*13*).

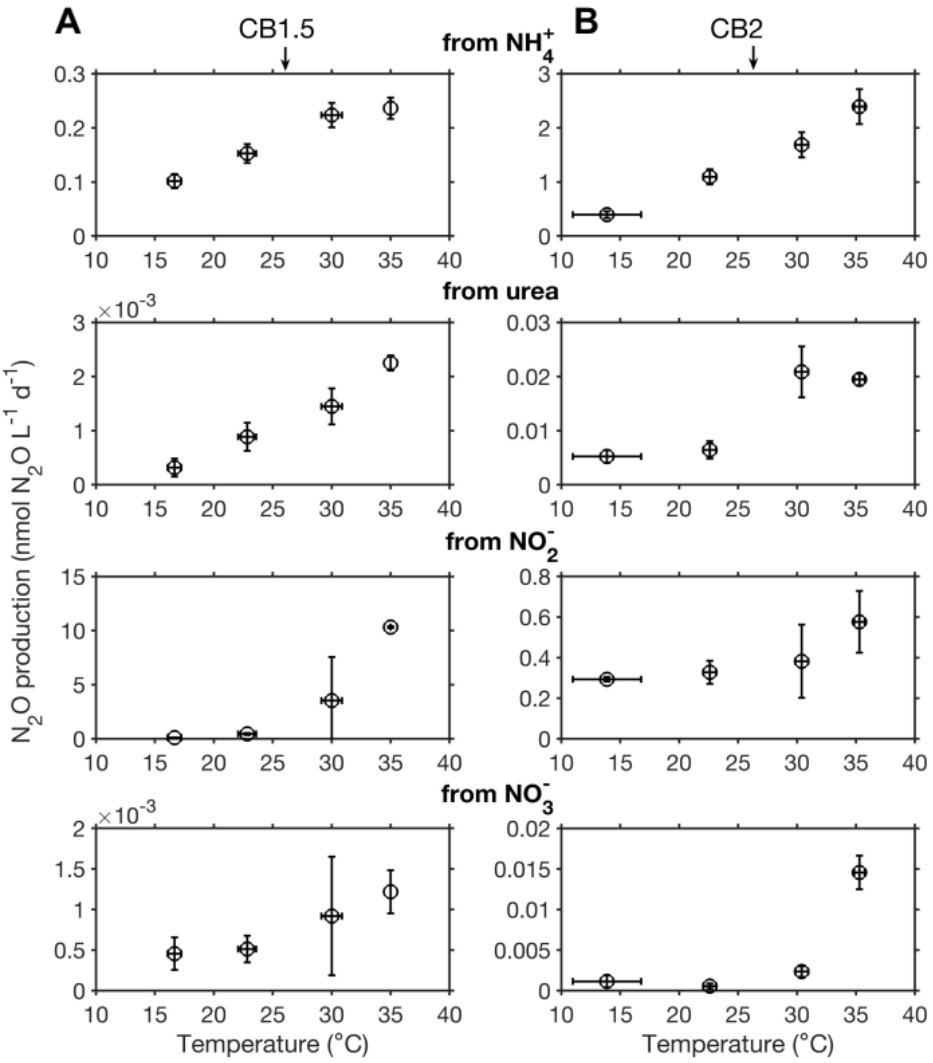


**Fig. S5. $N_2O$ production from four N substrates in response to the manipulated temperature changes for samples collected at stations CB1.5 (A) and CB2 (B).** Arrows on the top panels denote in-situ temperature at two stations. Vertical error bars represent the uncertainty of linear regression of $^{15}N$-$N_2O$ production during the incubation time course. Horizontal error bars represent variations of temperature during the incubations.

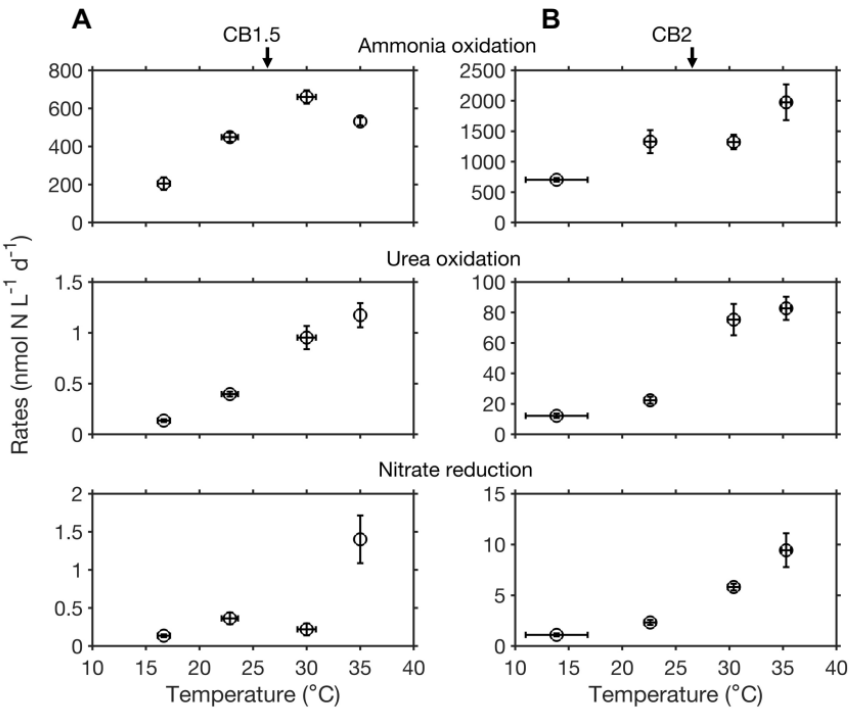


**Fig. S6. Nitrite production rate from nitrification (ammonia oxidation and urea oxidation) and denitrification (nitrate reduction) in response to manipulated temperature changes for samples collected at stations CB1.5 (A) and CB2 (B).** Arrows on the top panels denote in-situ temperature at two stations.

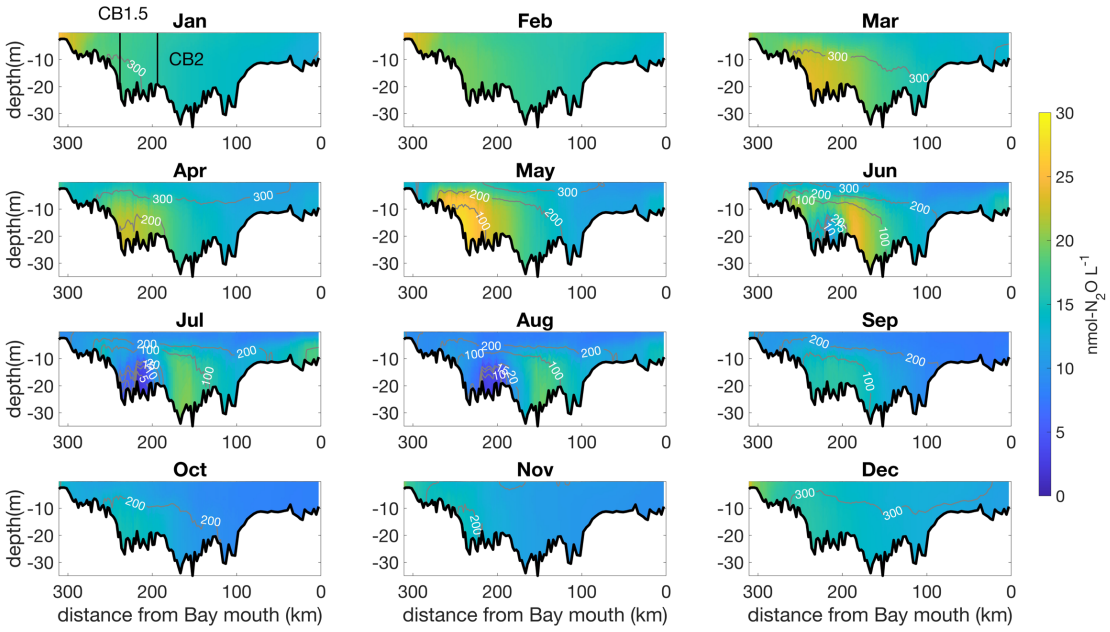


**Fig. S7. Transect of modeled monthly mean $N_2O$ concentrations from the Susquehanna River mouth to the Chesapeake Bay mouth in 2016.** Black contours with white numbers show the distribution of oxygen concentrations. Vertical black lines in Jan represent locations of stations CB1.5 and CB2.

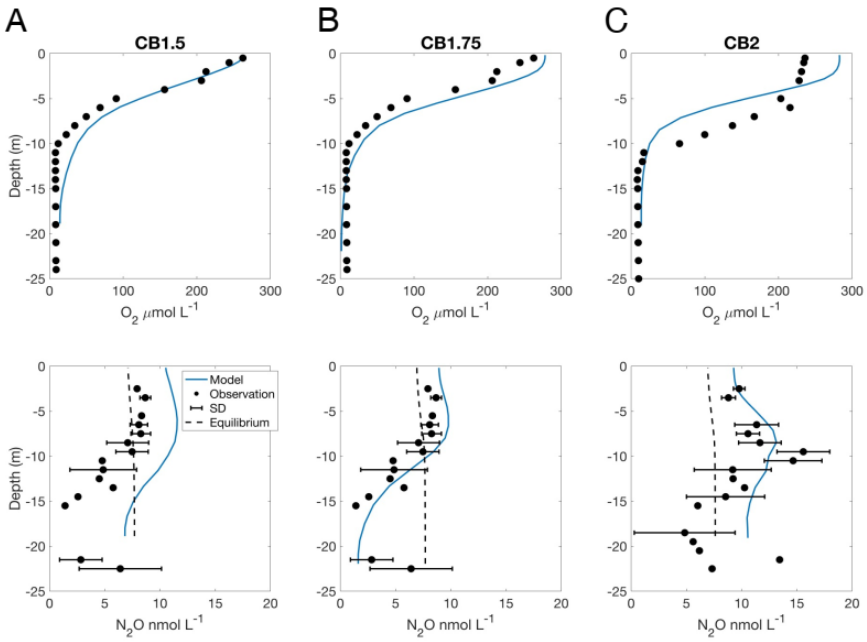


**Fig. S8. Comparison of observed and modeled depth profiles of oxygen and $N_2O$ concentrations at stations CB1.5 (A), CB1.75 (B), and CB2 (C) in the summer.** Locations of these stations are shown as vertical black lines in Fig. S12. Equilibrium $N_2O$ concentrations with the atmosphere are shown in black dashed lines. Note there is a temporal discrepancy between model results (monthly means of July in 2016) and observations (summer averages from observations conducted in 2013, 2016, 2020, and 2021).

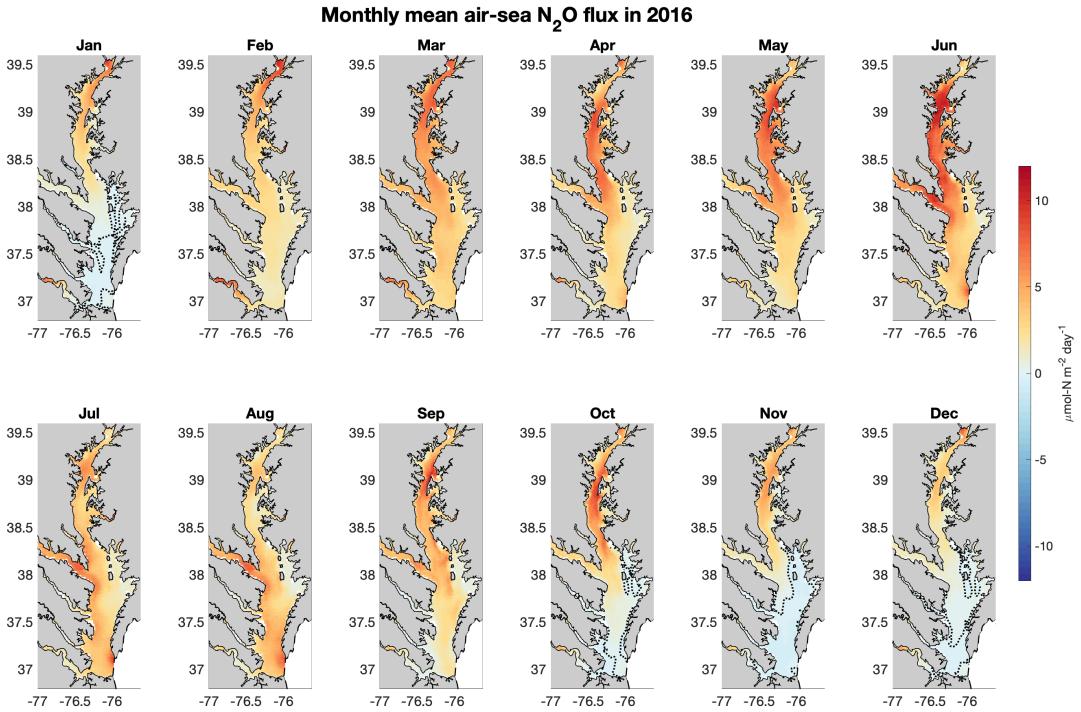


**Fig. S9. Modeled monthly mean air-sea $N_2O$ flux in Chesapeake Bay in 2016.**

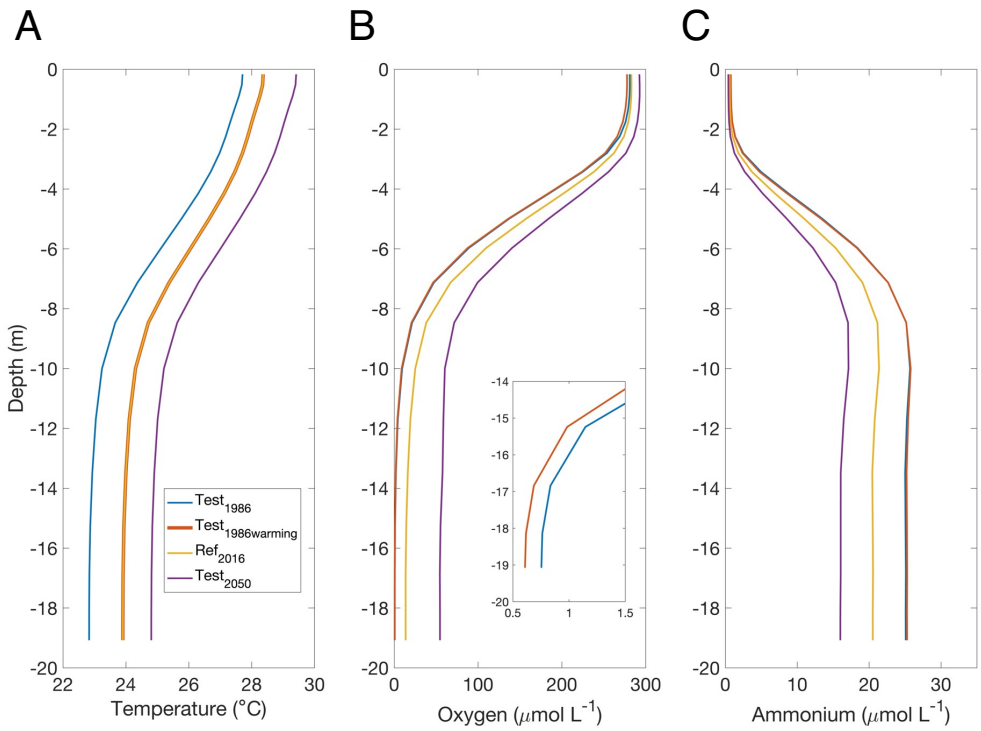


**Fig. S10. Vertical distributions of temperature (A), oxygen (B), ammonium concentrations (C) at station CB2 under four model simulation experiments.**

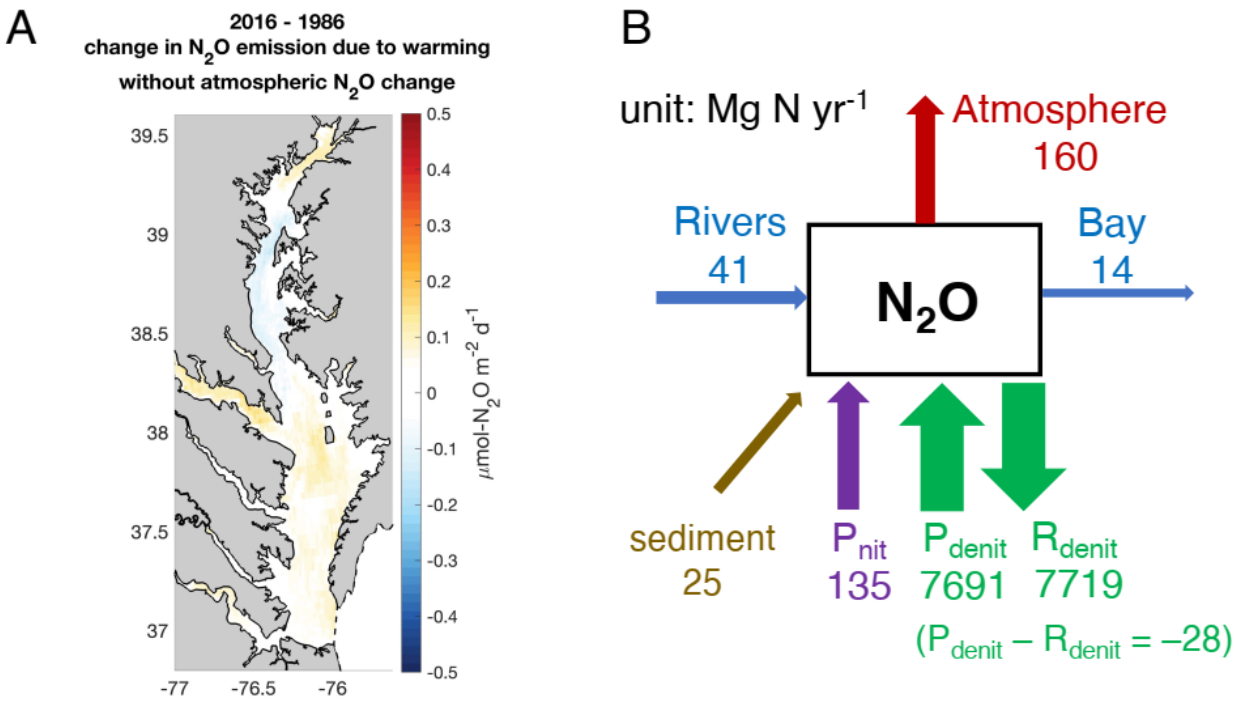


**Fig. S11. $N_2O$ flux change (A) and $N_2O$ budget (B) in 2016 under simulated warming from 1986 to 2016 without the increase in atmospheric $N_2O$ concentration.**

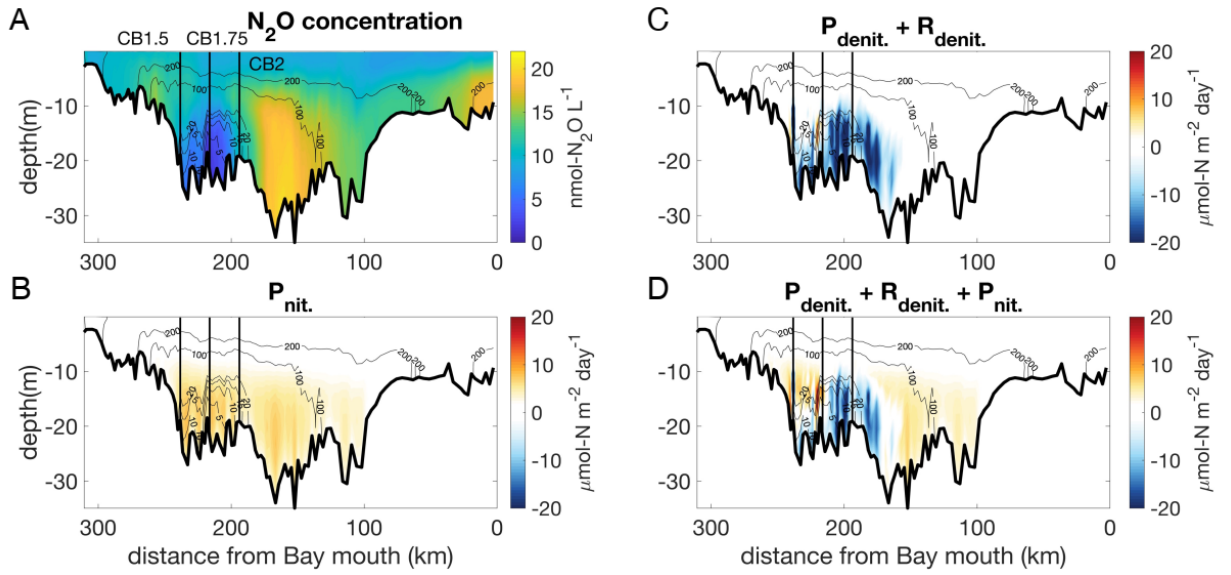


**Fig. S12. Transects of modeled mean $N_2O$ concentrations (A) and $N_2O$ cycling processes (B-D) from the Susquehanna River mouth to the Chesapeake Bay mouth in July 2016.** $N_2O$ cycling processes include $N_2O$ production from nitrification ($P_{nit}$), $N_2O$ production from denitrification ($P_{denit}$) and $N_2O$ reduction from denitrification ($R_{denit}$). Black contours show the distribution of oxygen concentrations.

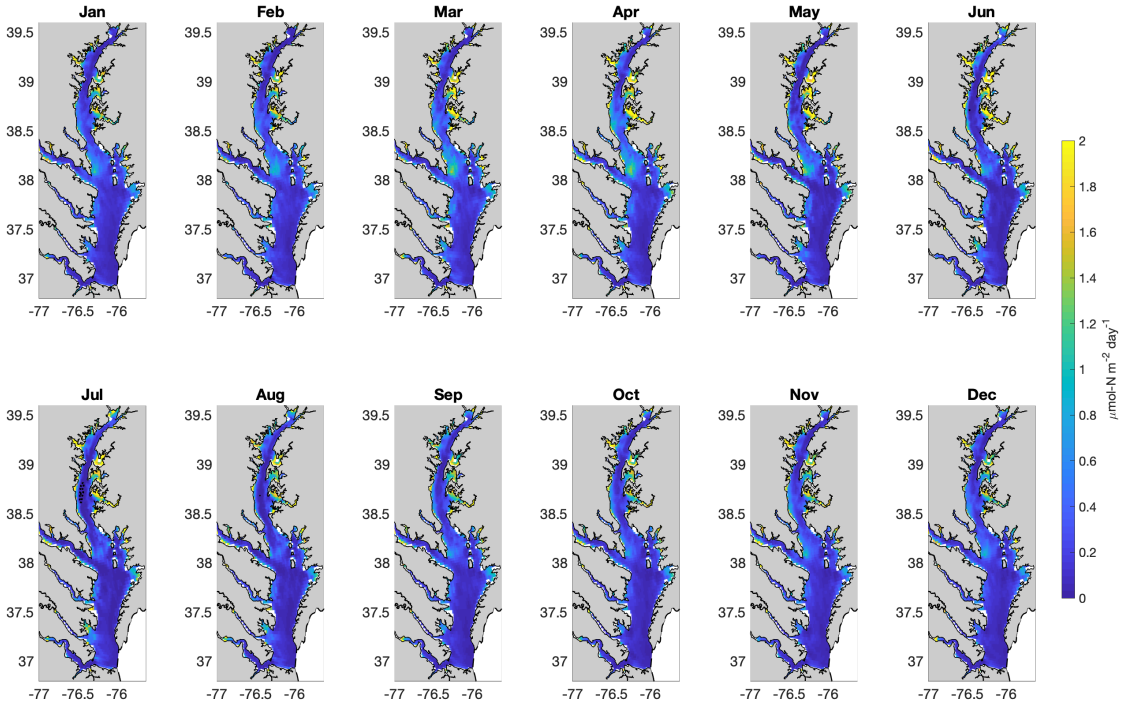


**Fig. S13. Modeled monthly variations in mean daily sedimentary $N_2O$ flux to the water column.**

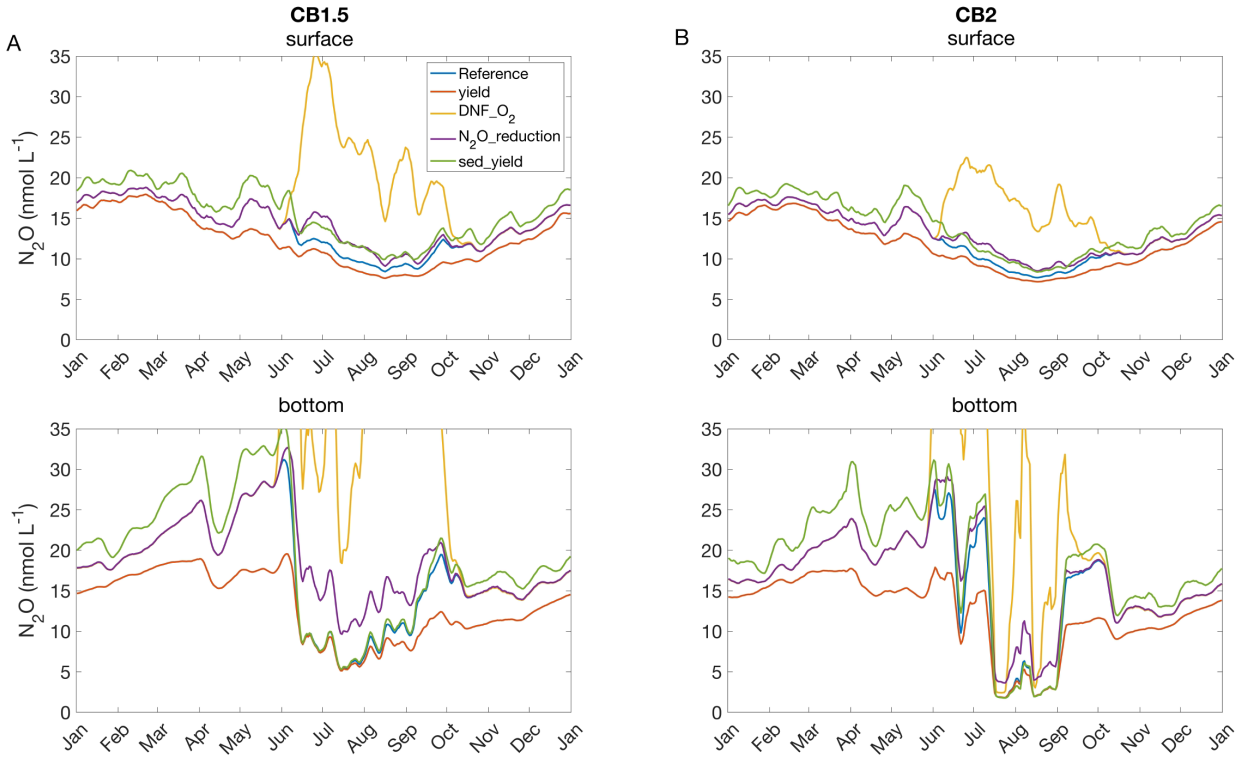


**Fig. S14. Modeled 7-day moving average of surface and bottom $N_2O$ concentrations at CB1.5 (A) and CB2 (B) in 2016 based on different model parameterizations (Table S9).** $N_2O$ concentrations in bottom water estimated under a high DNF_$O_2$ value are sometime beyond the range of y axes.

**Table S1. $Q_{10}$ of different $N_2O$ production processes.**

| Station | $N_2O$ production from | | | | Ammonia oxidation | Urea oxidation | Nitrate reduction |
|---|---|---|---|---|---|---|---|
| | $NH_4^+$ | Urea | $NO_2^-$ | $NO_3^-$ | | | |
| CB1.5 | 1.53 | 2.46 | 9.22 | 1.85 | 2.10 | 2.43 | 3.20 |
| CB2 | 2.04 | 1.93 | 1.41 | 2.39 | 1.51 | 2.28 | 2.85 |

**Table S2. Biogeochemical features of the incubation waters (ambient conditions for manipulation experiments).**

| Station | Depth (m) | Temperature (°C) | $O_2$ (µM) | Ammonium (µM) | Urea (µM) | Nitrite (µM) | Nitrate (µM) |
|---|---|---|---|---|---|---|---|
| CB1.5 | 7.19 | 26.03 | 10 | 7.75 | 0.44 | 0.6 | 0.19 |
| CB2 | 11.61 | 26.37 | 9.7 | 0.94 | 0.47 | 4.02 | 0.4 |

**Table S3. Oxygen concentration (µM) measured during oxygen manipulation experiments.**

| Target $O_2$ | CB1.5 7.19 m | | CB2 11.61 m | |
|---|---|---|---|---|
| | Ambient $O_2$ | Obtained $O_2$ | Ambient $O_2$ | Obtained $O_2$ |
| 0 | | 1.03±0.57 | | 0.46±0.07 |
| 2.5 | | 2.95±0.1 | | 1.94±0.15 |
| 5 | 10 | 4.88±0.4 | 9.7 | 5±0.01 |
| 10 | | 10.62±0.83 | | 10.51±0.18 |
| 20 | | 21.97±0.90 | | 21.21±0.37 |

**Table S4. Temperature (°C) measured during temperature manipulation experiments.**

| Target T | CB1.5 7.19 m | | CB2 11.61 m | |
|---|---|---|---|---|
| | Ambient T | Obtained T | Ambient T | Obtained T |
| 15 | 26.03 | 16.6±0.6 | 26.37 | 13.8±2.9 |
| 23 | | 22.8±0.7 | | 22.6±0.5 |
| 30 | | 30±0.8 | | 30.4±0.5 |
| 35 | | 35±0.1 | | 35.3±0.4 |

**Table S5. Equations for the water column of the biogeochemical module governing $N_2O$ in the ROMS-ECB.** Advective and diffusive terms are omitted for simplicity. The functions and parameters used in the table are further detailed in Table S6 and Table S7, respectively. Additional nitrogen cycling functions and parameters can be found in St-Laurent et al. 2020 (*30*). $N_2O$ in the model has units of mmol N $m^{-3}$, and t is in days.

| Variable (Symbol) | Term | Equation |
|---|---|---|
| Nitrous oxide ($N_2O$) mmol-N $m^{-3}$ | Rate of change = | $\partial N_2O/\partial t =$ |
| | + Nitrification (ammonium → $N_2O$) | $+ nf_{NTR} NH_4 \times N_2O_{yield}$ |
| | + Water column denitrif. (nitrate → $N_2O$) | $+ \eta_{DNF} f_{DNF} \exp(\psi_{N_2O} T) \times [(1 - \delta_N)(r_{SD} SD + r_{LD} LD) + r_{DON} DON_{SL}]$ |
| | – Water column denitrif. ($N_2O$ → $N_2$) | $- r_{N_2O\_DNF} \exp(\psi_{N_2O} T) \times f_{N_2O\_DNF} \times N_2O$ |
| | ± $N_2O$ exchange at air-sea interface | $+ 0.251 \div 100 \times 24 \times (\Delta z)^{-1} \times V_{wind}^2 \sqrt{660/Sc_{N2O}} \times (N_2O_{sat} \times pN_2O_{atm} \times 2 - N_2O)$ |
| | + Bottom denitrif. (nitrate → $N_2O$) | $+\gamma_{N_2O} \times [1 - (\eta_{NF/DNF} + \gamma_{DON})(1 + 3L_{BO2})] \times (1 - \phi_1)(\Delta z)^{-1} \times [w_P P(1 - \phi_2^P) + w_{SD} SD(1 - \phi_2^{SD}) + w_{LD} LD(1 - \phi_2^{LD})]$ |

**Table S6. Definition of functions used in $N_2O$ equations.**

| Symbol | Description | Equation | Unit |
|---|---|---|---|
| $N_2O_{yield}$ | $N_2O$ yield from nitrification (%) | $\frac{a}{O_2} + b$ | Dimensionless |
| $f_{DNF}$ | Limitation for anaerobic processes | $\frac{NO_3}{(NO_3 + K_{WNO_3})} \times \exp\left(-\frac{O_2}{K_{DNF}}\right)$ | Dimensionless |
| $f_{aero}$ | Limitation for aerobic processes | $\left[1 - \exp\left(-\frac{O_2}{K_{DNF}}\right)\right]$ | Dimensionless |
| $f_{N_2O\_DNF}$ | Limitation for $N_2O$ consumption via denitrification | $\exp\left(-\frac{O_2}{K_{N_2O}}\right)$ | Dimensionless |
| $Sc_{N_2O}$ | Schmidt number for $N_2O$ in seawater | See Wanninkhof (1992) (*73*) | Dimensionless |
| $N_2O_{sat}$ | $N_2O$ saturation in seawater | See Weiss & Price (1980) (*74*) | mol-$N_2O$/(L × atm) |

**Table S7. Definition of biogeochemical parameters used in $N_2O$ equations.**

| Symbol | Description (Name in Fortran code) | Value | Unit |
|---|---|---|---|
| $K_{DNF}$ | Oxygen sensitivity of $N_2O$ production via denitrification (K_DNF) | 3 | μM $O_2$ |
| $K_{N_2O}$ | Oxygen sensitivity of $N_2O$ consumption via denitrification (K_$N_2O$) | 2.33 | μM $O_2$ |
| $r_{N_2O\_DNF}$ | Rate constant of $N_2O$ consumption via denitrification ($N_2O$_DNF) | 120 | $day^{-1}$ |
| $\psi$ | Temperature-dependence for $N_2O$ cycling processes | 0.0875 | $℃^{-1}$ |
| a | Constant for $N_2O_{yield}$ | 0.3889 | dimensionless |
| b | Constant for $N_2O_{yield}$ | 0.2197 | dimensionless |
| $\gamma_{N_2O}$ | Fraction of $N_2O$ production via coupled nitrification/denitrification in sediment | $10^{-3}$ | dimensionless |
| $pN_2O_{atm}$ | Partial pressure of $N_2O$ in the air (2016) | 0.32933 | ppm by volume |

**Table S8. The list of numerical experiments conducted in this study.** Details of these model simulations can be found in Materials and Methods.

| Simulation | Atmospheric $N_2O$ | Atmospheric temperature | Riverine nutrient |
|---|---|---|---|
| *Ref* | 2016 | 2016 | 2016 |
| $Test_{1986}$ | 1986 | 1986: *Ref* + $\Delta\downarrow^{\#}$ in atmospheric temperature | 1986: *Ref* + $\Delta\uparrow^{\dagger}$ in riverine nutrient |
| $Test_{1986warming}$ | 2016 | 2016 | 1986: *Ref* + $\Delta\uparrow$ in riverine nutrient |
| $Test_{2050}$ | 2050 | 2050 | 2050: *Ref* + $\Delta\downarrow^{\&}$ from TMDL |

$^{\#}\Delta\downarrow$ refers to 30-year decrease in model forcings.

$^{\dagger}\Delta\uparrow$ refers to 30-year increase in model forcings.

$^{\&}\Delta\downarrow$ from TMDL refers to the decrease in riverine nutrient loading required by Total Maximum Daily Load (*28*).

**Table S9. Model sensitivity analysis with different parameterizations.**

| Simulation name | $N_2O\ yield_{nitrification}(\%) = \frac{a}{O_2} + b$ | $K_{DNF}$ (μM $O_2$) | $r_{N_2O\_DNF}$ ($day^{-1}$) | $\gamma_{N_2O}$ | Air-sea $N_2O$ flux (Mg N $yr^{-1}$)[&] |
|---|---|---|---|---|---|
| reference | a=0.3889; b=0.2197 | 3 | 120 | $10^{-3}$ | 140 |
| yield | a=0.3; b=0.08 | 3 | 120 | $10^{-3}$ | 79 |
| DNF_$O_2$ | a=0.3889; b=0.2197 | 5 | 120 | $10^{-3}$ | 204 |
| $N_2O$_reduction | a=0.3889; b=0.2197 | 3 | 60 | $10^{-3}$ | 148 |
| sed_yield | a=0.3889; b=0.2197 | 3 | 120 | $10^{-2}$ | 359 |
| half_$TMDL_{2050}$[#] | a=0.3889; b=0.2197 | 3 | 120 | $10^{-3}$ | 133 |

[&]Positive values indicate $N_2O$ outgassing to the atmosphere.

[#]This scenario assumes that only half of the TMDL goal is achieved by 2050. The fully achieved TMDL scenario ($Test_{2050}$) includes a bay-wide reduction in riverine nutrient loading of 28% from the reference run in 2016, setting the Bay watershed limit to 84.3 million kilograms of nitrogen (*28*). The half-achieved TMDL scenario (half_$TMDL_{2050}$) includes a 14% reduction in nutrient loading in 2050 compared to the reference run in 2016.

## REFERENCES AND NOTES


1. E. B. Barbier, S. D. Hacker, C. Kennedy, E. W. Koch, A. C. Stier, B. R. Silliman, The value of estuarine and coastal ecosystem services. *Ecol. Monogr.* **81**, 169–193 (2011).

2. A. Courrat, J. Lobry, D. Nicolas, P. Laffargue, R. Amara, M. Lepage, M. Girardin, O. Le Pape, Anthropogenic disturbance on nursery function of estuarine areas for marine species. *Estuar. Coast. Shelf Sci.* **81**, 179–190 (2009).

3. P. J. Statham, Nutrients in estuaries--an overview and the potential impacts of climate change. *Sci. Total Environ.* **434**, 213–227 (2012).

4. W. M. Kemp, W. R. Boynton, J. E. Adolf, D. F. Boesch, W. C. Boicourt, G. Brush, J. C. Cornwell, T. R. Fisher, P. M. Glibert, J. D. Hagy, L. W. Harding, E. D. Houde, D. G. Kimmel, W. D. Miller, R. I. E. Newell, M. R. Roman, E. M. Smith, J. C. Stevenson, Eutrophication of Chesapeake Bay: Historical trends and ecological interactions. *Mar. Ecol. Prog. Ser.* **303**, 1–29 (2005).

5. H. W. Paerl, L. M. Valdes, B. L. Peierls, J. E. Adolf, L. J. W. Harding, Anthropogenic and climatic influences on the eutrophication of large estuarine ecosystems. *Limnol. Oceanogr.* **51**, 448–462 (2006).

6. R. H. Murray, D. V. Erler, B. D. Eyre, Nitrous oxide fluxes in estuarine environments: response to global change. *Glob. Chang. Biol.* **21**, 3219–3245 (2015).

7. L. Y. Stein, Insights into the physiology of ammonia-oxidizing microorganisms. *Curr. Opin. Chem. Biol.* **49**, 9–15 (2019).

8. M. J. M. de Bie, J. J. Middelburg, M. Starink, H. J. Laanbroek, Factors controlling nitrous oxide at the microbial community and estuarine scale. *Mar. Ecol. Prog. Ser.* **240**, 1–9 (2002).

9. J. A. Rosentreter, G. G. Laruelle, H. W. Bange, T. S. Bianchi, J. J. M. Busecke, W.-J. Cai, B. D. Eyre, I. Forbrich, E. Y. Kwon, T. Maavara, N. Moosdorf, R. G. Najjar, V. V. S. S. Sarma, B. Van Dam, P. Regnier, Coastal vegetation and estuaries are collectively a greenhouse gas sink. *Nat. Clim. Chang.* **13**, 579–587 (2023).

10. H. W. Bange, S. Rapsomanikis, M. O. Andreae, Nitrous oxide in coastal waters. *Global Biogeochem. Cycles* **10**, 197–207 (1996).

11. H. Tian, R. Xu, J. G. Canadell, R. L. Thompson, W. Winiwarter, P. Suntharalingam, E. A. Davidson, P. Ciais, R. B. Jackson, G. Janssens-Maenhout, M. J. Prather, P. Regnier, N. Pan, S. Pan, G. P. Peters, H. Shi, F. N. Tubiello, S. Zaehle, F. Zhou, A. Arneth, G. Battaglia, S. Berthet, L. Bopp, A. F. Bouwman, E. T. Buitenhuis, J. Chang, M. P. Chipperfield, S. R. S. Dangal, E. Dlugokencky, J. W. Elkins, B. D. Eyre, B. Fu, B. Hall, A. Ito, F. Joos, P. B. Krummel, A. Landolfi, G. G. Laruelle, R. Lauerwald, W. Li, S. Lienert, T. Maavara, M. MacLeod, D. B. Millet, S. Olin, P. K. Patra, R. G. Prinn, P. A. Raymond, D. J. Ruiz, G. R. van der Werf, N. Vuichard, J. Wang, R. F. Weiss, K. C. Wells, C. Wilson, J. Yang, Y. Yao, A comprehensive quantification of global nitrous oxide sources and sinks. *Nature* **586**, 248–256 (2020).

12. Q. Ji, C. Frey, X. Sun, M. Jackson, Y.-S. Lee, A. Jayakumar, J. C. Cornwell, B. B. Ward, Nitrogen and oxygen availabilities control water column nitrous oxide production during seasonal anoxia in the Chesapeake Bay. *Biogeosciences* **15**, 6127–6138 (2018).

13. W. Tang, J. C. Tracey, J. Carroll, E. Wallace, J. A. Lee, L. Nathan, X. Sun, A. Jayakumar, B. B. Ward, Nitrous oxide production in the Chesapeake Bay. *Limnol. Oceanogr.* **67**, 2101–2116 (2022).

14. J. Zhou, Y. Zheng, L. Hou, Z. An, F. Chen, B. Liu, L. Wu, L. Qi, H. Dong, P. Han, G. Yin, X. Liang, Y. Yang, X. Li, D. Gao, Y. Li, Z. Liu, R. Bellerby, M. Liu, Effects of acidification on nitrification and associated nitrous oxide emission in estuarine and coastal waters. *Nat. Commun.* **14**, 1380 (2023).

15. E. Harris, E. Diaz-Pines, E. Stoll, M. Schloter, S. Schulz, C. Duffner, K. Li, K. L. Moore, J. Ingrisch, D. Reinthaler, S. Zechmeister-Boltenstern, S. Glatzel, N. Brüggemann, M. Bahn, Denitrifying pathways dominate nitrous oxide emissions from managed grassland during drought and rewetting. *Sci. Adv.* **7**, eabb7118 (2021).

16. E. Tan, W. Zou, Z. Zheng, X. Yan, M. Du, T.-C. Hsu, L. Tian, J. J. Middelburg, T. W. Trull, S.-J. Kao, Warming stimulates sediment denitrification at the expense of anaerobic ammonium oxidation. *Nat. Clim. Chang.* **10**, 349–355 (2020).

17. S. Li, A. Yue, S. S. Moore, F. Ye, J. Wu, Y. Hong, Y. Wang, Temperature-related $N_2O$ emission and emission potential of freshwater sediment. *Processes* **10**, 2728 (2022).

18. Y. Yao, H. Tian, H. Shi, S. Pan, R. Xu, N. Pan, J. G. Canadell, Increased global nitrous oxide emissions from streams and rivers in the Anthropocene. *Nat. Clim. Chang.* **10**, 138–142 (2020).

19. H. Tian, J. Yang, R. Xu, C. Lu, J. G. Canadell, E. A. Davidson, R. B. Jackson, A. Arneth, J. Chang, P. Ciais, S. Gerber, A. Ito, F. Joos, S. Lienert, P. Messina, S. Olin, S. Pan, C. Peng, E. Saikawa, R. L. Thompson, N. Vuichard, W. Winiwarter, S. Zaehle, B. Zhang, Global soil nitrous oxide emissions since the preindustrial era estimated by an ensemble of terrestrial biosphere models: Magnitude, attribution, and uncertainty. *Glob. Chang. Biol.* **25**, 640–659 (2019).

20. T. J. Griffis, Z. Chen, J. M. Baker, J. D. Wood, D. B. Millet, X. Lee, R. T. Venterea, P. A. Turner, Nitrous oxide emissions are enhanced in a warmer and wetter world. *Proc. Natl. Acad. Sci. U.S.A.* **114**, 12081–12085 (2017).

21. D. Breitburg, L. A. Levin, A. Oschlies, M. Grégoire, F. P. Chavez, D. J. Conley, V. Garçon, D. Gilbert, D. Gutiérrez, K. Isensee, G. S. Jacinto, K. E. Limburg, I. Montes, S. W. A. Naqvi, G. C. Pitcher, N. N. Rabalais, M. R. Roman, K. A. Rose, B. A. Seibel, M. Telszewski, M. Yasuhara, J. Zhang, Declining oxygen in the global ocean and coastal waters. *Science* **359**, eaam7240 (2018).

22. R. Varela, M. de Castro, J. M. Dias, M. Gomez-Gesteira, Coastal warming under climate change: Global, faster and heterogeneous. *Sci. Total Environ.* **886**, 164029 (2023).

23. F. P. Lima, D. S. Wethey, Three decades of high-resolution coastal sea surface temperatures reveal more than warming. *Nat. Commun.* **3**, 704 (2012).

24. S. P. Seitzinger, E. Mayorga, A. F. Bouwman, C. Kroeze, A. H. W. Beusen, G. Billen, G. Van Drecht, E. Dumont, B. M. Fekete, J. Garnier, J. A. Harrison, Global river nutrient export: A scenario analysis of past and future trends. *Glob. Biogeochem. Cycles* **24**, 2009GB003587 (2010).

25. R. R. Murphy, W. M. Kemp, W. P. Ball, Long-term trends in chesapeake bay seasonal hypoxia, stratification, and nutrient loading. *Estuaries Coasts* **34**, 1293–1309 (2011).

26. K. E. Hinson, M. A. M. Friedrichs, P. St-Laurent, F. Da, R. G. Najjar, Extent and causes of chesapeake bay warming. *J. Am. Water Resour. Assoc.* **58**, 805–825 (2022).

27. Q. Zhang, J. D. Blomquist, R. M. Fanelli, J. L. D. Keisman, D. L. Moyer, M. J. Langland, Progress in reducing nutrient and sediment loads to Chesapeake Bay: Three decades of monitoring data and implications for restoring complex ecosystems. *WIREs Water* **10**, e1671 (2023).

28. USEPA, Chesapeake Bay total maximum daily load for nitrogen, phosphorus, and sediment (USEPA, 2010).

29. L. T. Frankel, M. A. M. Friedrichs, P. St-Laurent, A. J. Bever, R. N. Lipcius, G. Bhatt, G. W. Shenk, Nitrogen reductions have decreased hypoxia in the Chesapeake Bay: Evidence from empirical and numerical modeling. *Sci. Total Environ.* **814**, 152722 (2022).

30. P. St-Laurent, M. A. M. Friedrichs, R. G. Najjar, E. H. Shadwick, H. Tian, Y. Yao, Relative impacts of global changes and regional watershed changes on the inorganic carbon balance of the Chesapeake Bay. *Biogeosciences* **17**, 3779–3796 (2020).

31. F. Da, M. A. M. Friedrichs, P. St-Laurent, E. H. Shadwick, R. G. Najjar, K. E. Hinson, Mechanisms driving decadal changes in the carbonate system of a coastal plain estuary. *J. Geophys. Res. Oceans* **126**, e2021JC017239 (2021).

32. A. F. Shchepetkin, J. C. McWilliams, The regional oceanic modeling system (ROMS): A split-explicit, free-surface, topography-following-coordinate oceanic model. *Ocean Model* **9**, 347–404 (2005).

33. L. Hink, P. Lycus, C. Gubry-Rangin, A. Frostegard, G. W. Nicol, J. I. Prosser, L. R. Bakken, Kinetics of $NH_3$-oxidation, NO-turnover, $N_2O$-production and electron flow during oxygen depletion in model bacterial and archaeal ammonia oxidisers. *Environ. Microbiol.* **19**, 4882–4896 (2017).

34. Q. Ji, A. R. Babbin, A. Jayakumar, S. Oleynik, B. B. Ward, Nitrous oxide production by nitrification and denitrification in the Eastern Tropical South Pacific oxygen minimum zone. *Geophys. Res. Lett.* **42**, 10755–10764 (2015).

35. Q. Ji, E. Buitenhuis, P. Suntharalingam, J. L. Sarmiento, B. B. Ward, Global nitrous oxide production determined by oxygen sensitivity of nitrification and denitrification. *Glob. Biogeochem. Cycles* **32**, 1790–1802 (2018).

36. A. E. Santoro, C. Buchwald, A. N. Knapp, W. M. Berelson, D. G. Capone, K. L. Casciotti, Nitrification and nitrous oxide production in the offshore waters of the eastern tropical south pacific. *Glob. Biogeochem. Cycles* **35**, e2020GB006716 (2021).

37. C. Nevison, J. H. Butler, J. W. Elkins, Global distribution of $N_2O$ and the $\Delta N_2O$-AOU yield in the subsurface ocean. *Glob. Biogeochem. Cycles* **17**, 2003GB002068 (2003).

38. X. Peng, C. A. Fuchsman, A. Jayakumar, S. Oleynik, W. Martens-Habbena, A. H. Devol, B. B. Ward, Ammonia and nitrite oxidation in the Eastern Tropical North Pacific. *Glob. Biogeochem. Cycles* **29**, 2034–2049 (2015).

39. N. J. Bouskill, D. Eveillard, D. Chien, A. Jayakumar, B. B. Ward, Environmental factors determining ammonia-oxidizing organism distribution and diversity in marine environments. *Environ. Microbiol.* **14**, 714–729 (2012).

40. J. Michael Beman, B. N. Popp, S. E. Alford, Quantification of ammonia oxidation rates and ammonia-oxidizing archaea and bacteria at high resolution in the Gulf of California and eastern tropical North Pacific Ocean. *Limnol. Oceanogr.* **57**, 711–726 (2012).

41. C. Frey, H. W. Bange, E. P. Achterberg, A. Jayakumar, C. R. Löscher, D. L. Arévalo-Martínez, E. León-Palmero, M. Sun, X. Sun, R. C. Xie, S. Oleynik, B. B. Ward, Regulation

of nitrous oxide production in low-oxygen waters off the coast of Peru. *Biogeosciences* **17**, 2263–2287 (2020).

42. A. Bourbonnais, B. X. Chang, R. E. Sonnerup, S. C. Doney, M. A. Altabet, Marine $N_2O$ cycling from high spatial resolution concentration, stable isotopic and isotopomer measurements along a meridional transect in the eastern Pacific Ocean. *Front. Mar. Sci.* **10**, 1137064 (2023).

43. Y. Zhang, J. Wang, S. Dai, Y. Sun, J. Chen, Z. Cai, J. Zhang, C. Müller, Temperature effects on $N_2O$ production pathways in temperate forest soils. *Sci. Total Environ.* **691**, 1127–1136 (2019).

44. Z.-Z. Zheng, L.-W. Zheng, M. N. Xu, E. Tan, D. A. Hutchins, W. Deng, Y. Zhang, D. Shi, M. Dai, S.-J. Kao, Substrate regulation leads to differential responses of microbial ammonia-oxidizing communities to ocean warming. *Nat. Commun.* **11**, 3511 (2020).

45. A. Canion, J. E. Kostka, T. M. Gihring, M. Huettel, J. E. E. van Beusekom, H. Gao, G. Lavik, M. M. M. Kuypers, Temperature response of denitrification and anammox reveals the adaptation of microbial communities to in situ temperatures in permeable marine sediments that span 50° in latitude. *Biogeosciences* **11**, 309–320 (2014).

46. A. J. Veraart, J. J. de Klein, M. Scheffer, Warming can boost denitrification disproportionately due to altered oxygen dynamics. *PLOS ONE* **6**, e18508 (2011).

47. S. M. Laperriere, N. J. Nidzieko, R. J. Fox, A. W. Fisher, A. E. Santoro, Observations of variable ammonia oxidation and nitrous oxide flux in a eutrophic estuary. *Estuaries Coasts* **42**, 33–44 (2019).

48. J. J. McCarthy, W. Kaplan, J. L. Nevins, Chesapeake Bay nutrient and plankton dynamics. 2. Sources and sinks of nitrite[1]. *Limnol. Oceanogr.* **29**, 84–98 (1984).

49. D. J. Conley, J. Carstensen, J. Aigars, P. Axe, E. Bonsdorff, T. Eremina, B. M. Haahti, C. Humborg, P. Jonsson, J. Kotta, C. Lannegren, U. Larsson, A. Maximov, M. R. Medina, E.

Lysiak-Pastuszak, N. Remeikaite-Nikiene, J. Walve, S. Wilhelms, L. Zillen, Hypoxia is increasing in the coastal zone of the Baltic Sea. *Environ. Sci. Technol.* **45**, 6777–6783 (2011).

50. S. Saraiva, H. E. Markus Meier, H. Andersson, A. Höglund, C. Dieterich, M. Gröger, R. Hordoir, K. Eilola, Baltic Sea ecosystem response to various nutrient load scenarios in present and future climates. *Clim. Dyn.* **52**, 3369–3387 (2019).

51. M. Dai, Y. Zhao, F. Chai, M. Chen, N. Chen, Y. Chen, D. Cheng, J. Gan, D. Guan, Y. Hong, J. Huang, Y. Lee, K. M. Y. Leung, P. E. Lim, S. Lin, X. Lin, X. Liu, Z. Liu, Y.-W. Luo, F. Meng, C. Sangmanee, Y. Shen, K. Uthaipan, W. I. A. Wan Talaat, X. S. Wan, C. Wang, D. Wang, G. Wang, S. Wang, Y. Wang, Y. Wang, Z. Wang, Z. Wang, Y. Xu, J.-Y. T. Yang, Y. Yang, M. Yasuhara, D. Yu, J. Yu, L. Yu, Z. Zhang, Z. Zhang, Persistent eutrophication and hypoxia in the coastal ocean. *Camb. Prism. Coast. Futures* **1**, e19 (2023).

52. H. Lin, M. Dai, S.-J. Kao, L. Wang, E. Roberts, J.-Y. T. Yang, T. Huang, B. He, Spatiotemporal variability of nitrous oxide in a large eutrophic estuarine system: The pearl river estuary China. *Mar. Chem.* **182**, 14–24 (2016).

53. X. S. Wan, H. X. Sheng, L. Liu, H. Shen, W. Tang, W. Zou, M. N. Xu, Z. Zheng, E. Tan, M. Chen, Y. Zhang, B. B. Ward, S. J. Kao, Particle-associated denitrification is the primary source of $N_2O$ in oxic coastal waters. *Nat. Commun.* **14**, 8280 (2023).

54. J. Syvitski, J. R. Ángel, Y. Saito, I. Overeem, C. J. Vörösmarty, H. Wang, D. Olago, Earth's sediment cycle during the Anthropocene. *Nat. Rev. Earth Environ.* **3**, 179–196 (2022).

55. S. C. Doney, D. S. Busch, S. R. Cooley, K. J. Kroeker, The impacts of ocean acidification on marine ecosystems and reliant human communities. *Annu. Rev. Environ. Resour.* **45**, 83–112 (2020).

56. R. M. Holmes, A. Aminot, R. Kérouel, B. A. Hooker, B. J. Peterson, A simple and precise method for measuring ammonium in marine and freshwater ecosystems. *Can. J. Fish. Aquat. Sci.* **56**, 1801–1808 (1999).

57. H. P. Hansen, F. Koroleff, "Determination of nutrients" in *Methods of Seawater Analysis* (WILEY-VCH Verlag GmbH, 1999), pp. 159–228.

58. L. Chen, J. Ma, Y. Huang, M. Dai, X. Li, Optimization of a colorimetric method to determine trace urea in seawater. *Limnol. Oceanogr. Methods* **13**, 303–311 (2015).

59. R. S. Braman, S. A. Hendrix, Nanogram nitrite and nitrate determination in environmental and biological materials by vanadium(III) reduction with chemiluminescence detection. *Anal. Chem.* **61**, 2715–2718 (1989).

60. A. Bourbonnais, C. Frey, X. Sun, L. A. Bristow, A. Jayakumar, N. E. Ostrom, K. L. Casciotti, B. B. Ward, Protocols for assessing transformation rates of nitrous oxide in the water column. *Front. Mar. Sci.* **8**, 611937 (2021).

61. J. A. Cram, A. Hollins, A. J. McCarty, G. Martinez, M. Cui, M. L. Gomes, C. A. Fuchsman, Microbial diversity and abundance vary along salinity, oxygen, and particle size gradients in the Chesapeake Bay. *Environ. Microbiol.* **26**, e16557 (2024).

62. W. Tang, S. G. Fortin, N. Intrator, J. A. Lee, M. A. Kunes, A. Jayakumar, B. B. Ward, Determination of site-specific nitrogen cycle reaction kinetics allows accurate simulation of in situ nitrogen transformation rates in a large North American estuary. *Limnol. Oceanogr.* **69**, 1757–1768 (2024).

63. C. C. Michiels, J. A. Huggins, K. E. Giesbrecht, J. S. Spence, R. L. Simister, D. E. Varela, S. J. Hallam, S. A. Crowe, Rates and pathways of $N_2$ production in a persistently anoxic Fjord: Saanich Inlet British Columbia. *Front. Mar. Sci.* **6**, 27 (2019).

64. M. Trimmer, P.-M. Chronopoulou, S. T. Maanoja, R. C. Upstill-Goddard, V. Kitidis, K. J. Purdy, Nitrous oxide as a function of oxygen and archaeal gene abundance in the North Pacific. *Nat. Commun.* **7**, 13451 (2016).

65. M. R. McIlvin, M. A. Altabet, Chemical conversion of nitrate and nitrite to nitrous oxide for nitrogen and oxygen isotopic analysis in freshwater and seawater. *Anal. Chem.* **77**, 5589–5595 (2005).

66. J. Wang, L. Vilmin, J. M. Mogollon, A. H. W. Beusen, W. J. van Hoek, X. Liu, P. A. Pika, J. J. Middelburg, A. F. Bouwman, Inland waters increasingly produce and emit nitrous oxide. *Environ. Sci. Technol.* **57**, 13506–13519 (2023).

67. Y. Feng, M. A. M. Friedrichs, J. Wilkin, H. Tian, Q. Yang, E. E. Hofmann, J. D. Wiggert, R. R. Hood, Chesapeake Bay nitrogen fluxes derived from a land-estuarine ocean biogeochemical modeling system: Model description, evaluation, and nitrogen budgets. *J. Geophys. Res. Biogeosci.* **120**, 1666–1695 (2015).

68. I. D. Irby, M. A. M. Friedrichs, F. Da, K. E. Hinson, The competing impacts of climate change and nutrient reductions on dissolved oxygen in Chesapeake Bay. *Biogeosciences* **15**, 2649–2668 (2018).

69. F. Da, M. A. M. Friedrichs, P. St-Laurent, Impacts of atmospheric nitrogen deposition and coastal nitrogen fluxes on oxygen concentrations in Chesapeake Bay. *J. Geophys. Res. Oceans* **123**, 5004–5025 (2018).

70. J. S. Turner, P. St-Laurent, M. A. M. Friedrichs, C. T. Friedrichs, Effects of reduced shoreline erosion on Chesapeake Bay water clarity. *Sci. Total Environ.* **769**, 145157 (2021).

71. K. E. Hinson, M. A. M. Friedrichs, R. G. Najjar, M. Herrmann, Z. Bian, G. Bhatt, P. St-Laurent, H. Tian, G. Shenk, Impacts and uncertainties of climate-induced changes in watershed inputs on estuarine hypoxia. *Biogeosciences* **20**, 1937–1961 (2023).

72. W. Tang, A. Jayakumar, X. Sun, J. C. Tracey, J. Carroll, E. Wallace, J. A. Lee, L. Nathan, B. Ward, Nitrous oxide consumption in oxygenated and anoxic estuarine waters. *Geophys. Res. Lett.* **49**, e2022GL100657 (2022).

73. R. Wanninkhof, Relationship between wind speed and gas exchange over the ocean. *J. Geophys. Res. Oceans* **97**, 7373–7382 (1992).

74. R. F. Weiss, B. A. Price, Nitrous oxide solubility in water and seawater. *Mar. Chem.* **8**, 347–359 (1980).

75. H. Hersbach, B. Bell, P. Berrisford, S. Hirahara, A. Horányi, J. Muñoz-Sabater, J. Nicolas, C. Peubey, R. Radu, D. Schepers, A. Simmons, C. Soci, S. Abdalla, X. Abellan, G. Balsamo, P. Bechtold, G. Biavati, J. Bidlot, M. Bonavita, G. De Chiara, P. Dahlgren, D. Dee, M. Diamantakis, R. Dragani, J. Flemming, R. Forbes, M. Fuentes, A. Geer, L. Haimberger, S. Healy, R. J. Hogan, E. Hólm, M. Janisková, S. Keeley, P. Laloyaux, P. Lopez, C. Lupu, G. Radnoti, P. de Rosnay, I. Rozum, F. Vamborg, S. Villaume, J. N. Thépaut, The ERA5 global reanalysis. *Q. J. R. Meteorol. Soc.* **146**, 1999–2049 (2020).

76. A. J. Bever, M. A. M. Friedrichs, P. St-Laurent, Real-time environmental forecasts of the Chesapeake Bay: Model setup, improvements, and online visualization. *Environ. Model. Softw.* **140**, 105036 (2021).

77. H. Tian, Q. Yang, R. G. Najjar, W. Ren, M. A. M. Friedrichs, C. S. Hopkinson, S. Pan, Anthropogenic and climatic influences on carbon fluxes from eastern North America to the Atlantic Ocean: A process-based modeling study. *J. Geophys. Res. Biogeosciences* **120**, 757–772 (2015).

78. CBP, Online draft documentation for Phase 6 modeling tools (2017).

79. W. Tang, J. Talbott, T. Jones, B. B. Ward, Variable contribution of wastewater treatment plant effluents to downstream nitrous oxide concentrations and emissions. *Biogeosciences* **21**, 3239–3250 (2024).

80. A. Freing, D. W. R. Wallace, T. Tanhua, S. Walter, H. W. Bange, North Atlantic production of nitrous oxide in the context of changing atmospheric levels. *Glob. Biogeochem. Cycles* **23**, 2009GB003472 (2009).

81. C. R. Schwalm, S. Glendon, P. B. Duffy, RCP8.5 tracks cumulative $CO_2$ emissions. *Proc. Natl. Acad. Sci. U.S.A.* **117**, 19656–19657 (2020).

82. K. Riahi, S. Rao, V. Krey, C. Cho, V. Chirkov, G. Fischer, G. Kindermann, N. Nakicenovic, P. Rafaj, RCP 8.5—A scenario of comparatively high greenhouse gas emissions. *Clim. Change* **109**, 33–57 (2011).

83. E. Tan, T. C. Hsu, W. Zou, X. Yan, Z. Huang, B. Chen, Y. Chang, Z. Zheng, L. Zheng, M. Xu, L. Tian, S. J. Kao, Quantitatively deciphering the roles of sediment nitrogen removal in environmental and climatic feedbacks in two subtropical estuaries. *Water Res.* **224**, 119121 (2022).

84. S. Q. Foster, R. W. Fulweiler, Sediment nitrous oxide fluxes are dominated by uptake in a temperate estuary. *Front. Mar. Sci.* **3**, 40 (2016).

85. J. J. Beaulieu, J. L. Tank, S. K. Hamilton, W. M. Wollheim, R. O. Hall Jr., P. J. Mulholland, B. J. Peterson, L. R. Ashkenas, L. W. Cooper, C. N. Dahm, W. K. Dodds, N. B. Grimm, S. L. Johnson, W. H. McDowell, G. C. Poole, H. M. Valett, C. P. Arango, M. J. Bernot, A. J. Burgin, C. L. Crenshaw, A. M. Helton, L. T. Johnson, J. M. O'Brien, J. D. Potter, R. W. Sheibley, D. J. Sobota, S. M. Thomas, Nitrous oxide emission from denitrification in stream and river networks. *Proc. Natl. Acad. Sci. U.S.A.* **108**, 214–219 (2011).

86. S. P. Seitzinger, Denitrification in freshwater and coastal marine ecosystems: Ecological and geochemical significance. *Limnol. Oceanogr.* **33**, 702–724 (1988).

87. R. R. Murphy, J. Keisman, J. Harcum, R. R. Karrh, M. Lane, E. S. Perry, Q. Zhang, Nutrient improvements in Chesapeake Bay: Direct effect of load reductions and implications for coastal management. *Environ. Sci. Technol.* **56**, 260–270 (2022).

88. C. Oviatt, L. Smith, J. Krumholz, C. Coupland, H. Stoffel, A. Keller, M. C. McManus, L. Reed, Managed nutrient reduction impacts on nutrient concentrations, water clarity, primary production, and hypoxia in a north temperate estuary. *Estuar. Coast. Shelf Sci.* **199**, 25–34 (2017).

89. M. B. McElroy, J. W. Elkins, S. C. Wofsy, C. E. Kolb, A. P. Durán, W. A. Kaplan, Production and release of $N_2O$ from the Potomac Estuary [1]. *Limnol. Oceanogr.* **23**, 1168–1182 (1978).

90. D. Bianchi, D. McCoy, S. Yang, Formulation, optimization, and sensitivity of NitrOMZv1.0, a biogeochemical model of the nitrogen cycle in oceanic oxygen minimum zones. *Geosci. Model Dev.* **16**, 3581–3609 (2023).